CORROSION SCIENCE AND TECHNOLOGY, Vol.20, No.4(2021), pp.175~182
[Research Article]
pISSN 1598-6462 / eISSN 2288-6524
DOI: https://doi.org/10.14773/cst.2021.20.4.175

A Study on the Corrosion Behavior of Magnesium Alloy Sealed with Chemical Conversion Coating and Sol-gel Coating

Dong Uk Lee, Shivshankar Chaudhari, Seung Yong Choi, Myung Jun Moon, and Min Young Shon†

Department of Industrial Chemistry, Pukyong National University, Busan, 48547, Republic of Korea
(Received March 27, 2020; Revised June 17, 2021; Accepted June 23, 2021)

Magnesium alloy is limited in the industrial field because its standard electrode potential is –2.363 V vs. NHE (Normal Hydrogen Electrode) at 25 °C. This high electrochemical activity causes magnesium to quickly corrode with oxygen in air; chemical conversion coating prevents corrosion but causes surface defects like cracks and pores. We have examined the anti-corrosion effect of sol-gel coating sealed on the defected conversion coating layer. Sol-gel coatings produced higher voltage current and smaller pore than the chemical conversion coating layer. The conversion coating on magnesium alloy AZ31 was prepared using phosphate-permanganate solution. The sol-gel coating was designed using trimethoxymethylsilane (MTMS) and (3-Glycidyloxypropyl) trimethoxysilane (GPTMS) as precursors, and aluminum acetylacetonate as a ring-opening agent. The thermal shock resistance was tested by exposing specimens at 140 °C in a convection oven; the results showed changes in the magnesium alloy AZ31 surface, such as oxidization and cracking. Scanning electron microscope (FE-SEM) analysis confirmed a sealed sol-gel coating layer on magnesium alloy AZ31. Electrochemical impedance spectroscopy (EIS) measured the differences in corrosion protection properties by sol-gel and conversion coatings in 0.35 wt% NaCl solution, and the potentiodynamic polarization test and confirmed conversion coating with the sol-gel coating show significantly improved resistance by crack sealing.

Keywords: *Sol-gel coating, EIS, Chemical conversion coating, Polarization test, Thermal shock test*

1. Introduction

The low density and high specific stiffness of magnesium-based alloys make them attractive for the aerospace and automobile industries, although they must be resisted due to their susceptibility to galvanic corrosion due to their highly negative electrochemical potential compared to other metals alloy [1]. In particular, magnesium alloys have been employ as a promising engine block material in the automotive industry [2,3]. Nevertheless, it is associated with an issue of galvanic corrosion in the engine block by the coolant, which can limit the use of magnesium alloy in engine blocks [4,5].

Therefore in that context, chemical conversion coating has been a traditionally used method for preventing corrosion of magnesium alloy. But, chemical conversion coating has chronic trouble, such as the occurrence of cracks and pores. And formed cracks and pores in chemical conversion coating reduces its anti-corrosion effect due to the formation of a free path through which corrosion factors can easily penetrate to the inner metal surface [6,7].

Sol-gel coatings consist of the application of thin silica film at the surfaces that can be deal with the defects formed in the conversion coating layer. Additionally, the sol-gel coating is an environmentally friendly process, needs a mild synthetic temperature, and a high voltage current creates quite a smaller pore than conversion coatings [8-10]. As sol-gel coating can minimize the coating defects formed in chemical conversion and dual-layer by sol-gel coated on chemical-conversion coating expects to shield an effect from the corrosion factor penetration [11-13].

Therefore, in this study, an application of chemical conversion coating and sol-gel coating dual-layer for

†Corresponding author: myshon@pknu.ac.kr
PhD candidate, Shivshankar Chaudhari: Researcher, Seung Yong Choi: master student', Myung Jun Moon: Professor, Min Young Shon: Professor

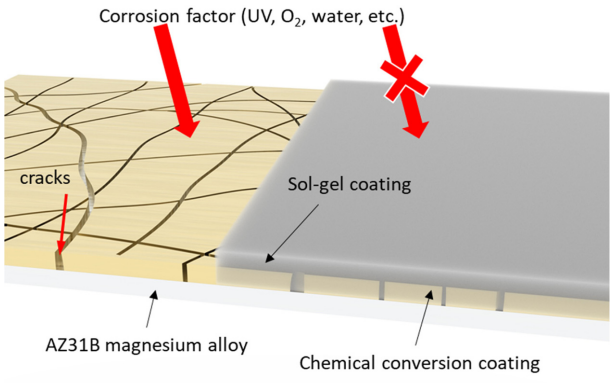

Fig. 1. The schematic illustration of dual chemical conversion and sol-gel coating on AZ31B magnesium alloy

protecting the substrate from corrosion factors has been investigated (Fig. 1). Chemical conversion coating was made from phosphate/permanganate layer, and sol-gel coating solution made by the sol-gel method consists of silicon and aluminum sol. Chemical conversion and sol-gel coated magnesium specimens were treated with a thermal shock test to assess thermal resistance for overcoming limitations in engine blocks. The electrochemical properties of coating layers were studied by EIS techniques.

2. Experimental Methods

2.1. Chemicals

Sodium phosphate dibasic anhydrous (Na_2HPO_4, DSP, 99%), phosphoric acid (H_3PO_4, 85%) and sodium hydroxide (NaOH, 97%) were purchased from Dae-Jung chemicals (Korea). Sodium dodecyl sulfate (SDS, 34.5%), oxalic acid (99.5%) and sodium chloride (NaCl, 99.5%) were obtained from Junsei Chem. Potassium permanganate ($KMnO_4$, 97%), 2-propanol anhydrous (IPA, 99.5%), trimethoxy-methylsilane (MTMS, 95%), (3-Glycidyloxypropyl) trime-thoxysilane (GPTMS, 98%), aluminum tri-sec butoxide (ATSB, 97%), acetylacetone (acac, 99%) were purchased from Sigma-Aldrich (USA). All chemicals were used without further purification.

2.2. Substrate preparation and coating procedure

For the synthesis of sol-gel coating, a solution from GPTMS, MTMS, ATSB, IPA, acac, and distilled water with a molar ratio of 0.5:1:0.28:3.4:0.18:10 was prepared and mixed using a magnetic stirrer. GPTMS, MTMS, and aluminum acetylacetonate, ATSB were used as a precursor and ring-opening agent, respectively. Sol-gel synthesis is a one-pot process performed at 80 ºC for 2 hours, and then the temperature was set to 60 ºC and continually stirred for 12 hours. The obtained pale yellow color product from sol-gel solution was aged for 1 day and used for coating Magnesium alloy. Magnesium alloy, which is commercial AZ31B, consist of Al 2.47%, Zn 0.93%, Mn 0.33%, Si 0.17%, F 1.47% and Mg 94.63% measured by EDS. Magnesium alloy specimens were steadily polished with 400, 600, and 1000 grit sandpaper until approximately 0.3 μm surface roughness was formed and then washed sufficiently with distilled water. Thereafter, it dried at 150 ºC by hot air with a heating gun and followed by washing with 1M KOH solution at room temperature for 2 minutes. Immediately, specimens were immersed into oxalic acid solution (1.0 g/L) for 30 seconds. Oxalic acid-treated magnesium alloy was thoroughly washed with DI water and dried by a heating gun with hot air at 150 ºC. The preparation of the chemical conversion coating solution was made by mixing DSP 150 g/L, $KMnO_4$ 40 g/L, SDS 0.8 g/L solutions, and phosphoric acid were added until the pH of the solution down to 5.5. After that, the solution temperature kept to 55 ºC. The chemical conversion coating layer was prepared by immersed a magnesium alloy abovementioned chemical conversion coating solution for 5 minutes at 55 ºC. The sol-gel coating was bar-coated using a No. 24 bar coater on the chemical conversion coated specimen and cured at 80 ºC for 1 hour. The thickness of the chemical conversion coating layer and sol-gel coating layer thickness was approximately 1 μm and 10 μm, respectively.

2.3. Thermal shock test

Firstly, all specimens were immersed in cold water for 10 min at 0 ºC, after that exposed to hot air condition (140 ºC) for 10 minutes. This process has been repeated 10 times. The surface changes of specimens under thermal shock tests were observed by scanning electron microscopy (SEM).

2.4. Scanning electron microscope and energy dispersive X-ray spectrometer.

Surface morphology of coatings and magnesium alloy composition were measured by Scanning electron microscope (FE-SEM, MIRA3, TESCAN, Czech). Surface

scanned with 5.0 kV of accelerating voltage and 3000 times of magnitudes. The cross-section was measured after the specimen was polished and molded with epoxy resin.

2.5. Fourier transform infrared spectroscopy (FTIR-ATR mode)

To determine the changes in the surface of the coatings, ATR-FTIR spectroscopy (iS10, Thermo Fisher Scientific, USA) was performed using a ZnSe crystal kit. Each specimen was washed with ethanol, dried with N2 gas, and analyzed over 32 scans with a resolution of 4 cm^{-1}, providing spectra in the range of 650–4000 cm^{-1}.

2.6. Electrochemical measurements

Electrochemical impedance spectroscopy (EIS) measurements performed with a computer-controlled EIS instrument (biologic sp240), and potentiodynamic polarization tests were performed by (EG&G Princeton applied research parstat2273). Each specimen was measured EIS after conducted the thermal shock test. The cell consists of three electrodes, a saturated calomel electrode (SCE) as a reference electrode, a carbon electrode as a counter electrode, and each specimen as a working electrode. All the tests were performed with 0.35 wt% NaCl electrolyte solution, and the working area of specimens exposed to the solution was 9.7 cm^2. EIS spectra were acquired in the frequency range from 100 kHz to 10 mHz with an AC wave of 100 mV. All measurements were accomplished at room temperature in a Faraday.

3. Results & discussion

3.1. Characterization of sol-gel coating

The FTIR (ATR mode) spectrum of the sol-gel sealed specimen is shown in Fig. 2a. Fig. 2a depicts that, broad peak at vibrational frequency 3418 cm^{-1} corresponds to the hydroxyl stretching from the GPTMS and siloxane moieties. Aliphatic asymmetry vibrations of the CH_3 group were observed at frequencies of 2971 and 2884 cm^{-1}, respectively. Si-CH_3 of MTMS has an asymmetric deformation vibration band at 1270 cm^{-1}, and siloxane in the sol-gel coating has two bands at 1111 and 1050 cm^{-1}, respectively, which can be seen in the spectrum. Based on the presence of FT-IR peak corresponds to the silicon-related functionality confirmed magnesium alloy specimen was well coated by sol-gel coating.

Fig. 2b shows XRD spectra of chemical conversion coating and sol-gel sealed specimen. Pure magnesium specimen and chemical conversion coating have almost the same XRD spectrum due to the deposition of the very thin chemical conversion coating. However, in sol-gel sealed specimen, the amorphous XRD peaks of silicon, as well as siloxane, appeared on the surface. This is further confirmed the successful deposition of sol-gel coating at the Mg alloy surface.

3.2. Thermal shock test

The result of the thermal shock test, as shown in Fig. 3. The SEM image clearly shows that even after the chemical

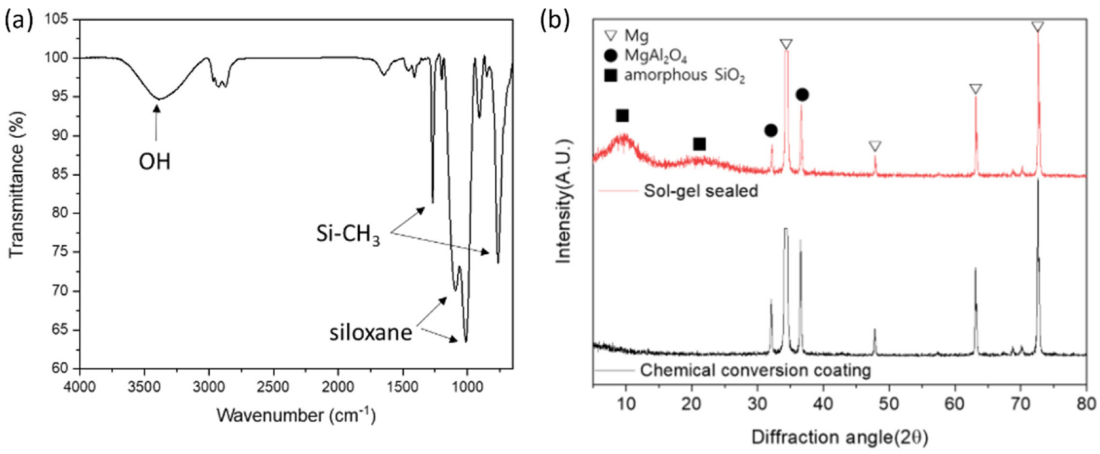

Fig. 2. (a) FT-IR spectrum of sol-gel sealed coating surface and (b) XRD spectra of sol-gel sealed coating and chemical conversion coating

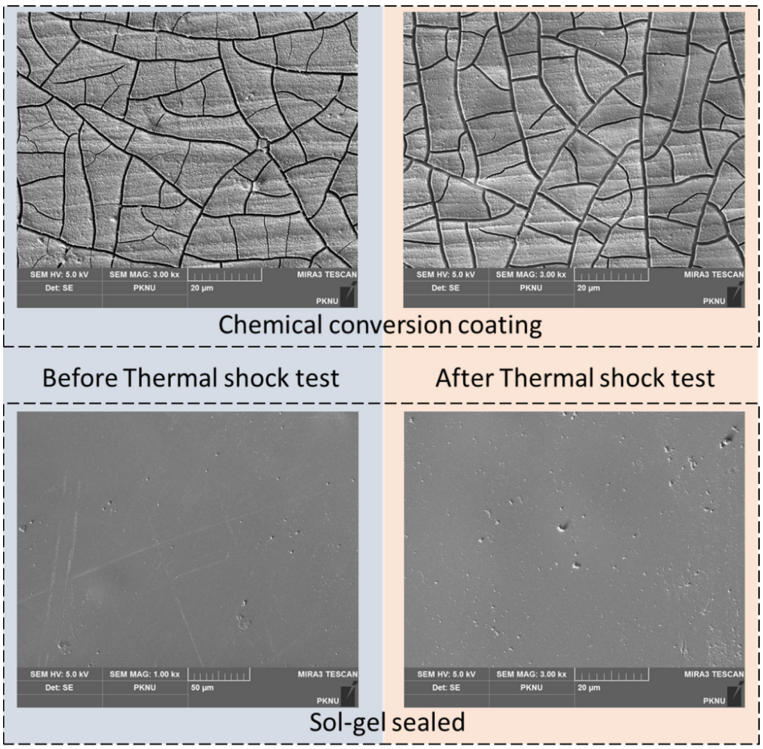

Fig. 3. The SEM image of chemical conversion coating and sol-gel sealed specimens with thermal shock test

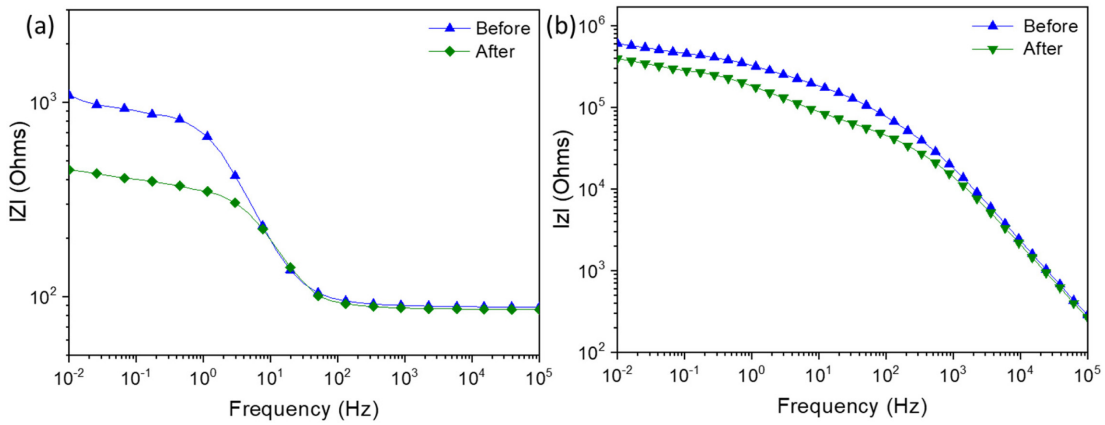

Fig. 4. Bode plots of (a) chemical conversion coating and (b) Sol-gel sealed specimens before and after thermal shock test

conversion coating, the Mg alloy has cracks and pores, and on thermal shock test after 10 times cycle of thermal shock test, it became more extensive. Therefore metal surfaces can be easily exposed to corrosion factors. But, on the other hand, it can clearly be seen from the SEM micrographs of sol-gel sealed coating specimen that the surface is dense and uncracked surface and even though, after 10 cycles of thermal shock test. The integrity of the coating was well maintained as there is no obvious existence of any void or crack.

3.3. EIS analysis of specimen after thermal shock test

Electrochemical impedance spectra obtained through the bode plots for the chemical conversion coating and sol-gel sealed coating specimens have depicted in Fig. 4. The conversion coating has an impedance of about 1.08×10^3 ohms before the thermal shock test; however, it significantly decreased to ~ 4.49×10^2 ohms due to thermal shock. In contrast, the sol-gel sealed specimen

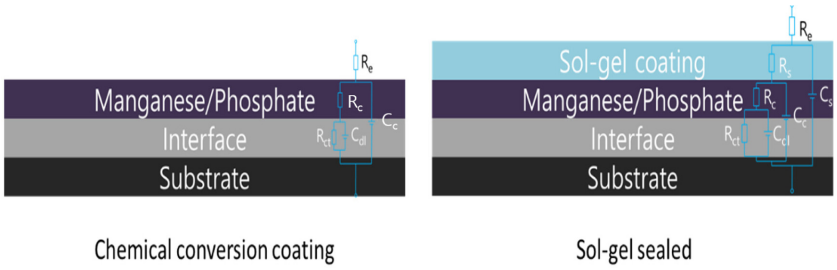

Fig. 5. The schematic illustration of electrical circuit components of each coating specimens

Table 1. The electrical equivalent circuit components of specimens

Specimen	Thermal shock test	R_e (Ω)	C_s (F)	R_s (Ω)	C_c (F)	R_c (Ω)	C_{dl} (F)	R_{ct} (Ω)
Chemical conversion coating	Before	88.7			1.68×10^{-4}	824.5	6.08×10^{-2}	114.8
	After	82.4			1.15×10^{-4}	290.4	1.80×10^{-2}	82.41
Sol-gel sealed	Before	100.2	3.26×10^{-8}	2.47×10^{5}	4.78×10^{-7}	4.66×10^{5}	3.77×10^{-5}	2.63×10^{5}
	After	102.8	1.82×10^{-8}	6.65×10^{4}	7.13×10^{-7}	3.13×10^{5}	2.41×10^{-5}	2.55×10^{5}

has a more high impedance of about 6.00×10^5 ohms before the thermal shock test and after the thermal shock test, marginally decreased impedance comparatively less to that of conversion coated specimen was observed. Therefore it is confirmed from the impedance of the bode plot that sol-gel sealed coating significantly improves the protection of metal substrate from the corrosion factor penetration. The components of the equivalent electrical circuit (Fig. 5) used for numerical fitting shown in Table 1 are described as R_e is the resistance of electrolyte; R_c is the resistance of chemical conversion coating; C_c is the capacitance of chemical conversion coating; R_s is the resistance of the sol-gel coating; C_s is the capacitance of sol-gel coating; R_{ct} is a resistance of charge transfer in the interface; C_{dl} is the capacitance of electrical double layer in the interface. In the beginning, the chemical conversion coating layer showed very poor impedance due to cracks and pores developed in a layer was observed. Although sol-gel sealed specimens have high impedance at R_s components, the chemical conversion coating layer at R_c component also showed very high impedance values. R_c value demonstrates that the sol-gel coating solution penetrated the chemical conversion coating and sealed the cracks and pores. Furthermore, even only sol-gel coating was more thickened, but the dual layer of sol-gel sealed with conversion coating (R_c) showed higher impedance than the only conversion coating observed.

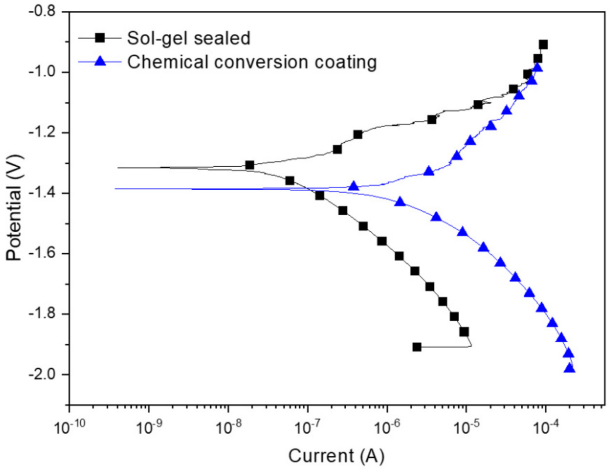

Fig. 6. The results of the potentiodynamic polarization test of specimens

3.4. Polarization curve results after thermal shock test

Fig. 6 shows polarization curves of conversion coating, sol-gel sealed specimen. The corrosion current densities (I_{corr}) and the corrosion potential (E_{corr}) were obtained from the polarization curves by the Tafel plot [14,15]. A Tafel plot have performed by anodically and cathodically polarizing the specimen from the corrosion potential (E_{corr}). The corrosion current density (I_{corr}) is obtained from a Tafel plot by extrapolating the intersection point to E_{corr}.

The corrosion potential is the potential at which the current of oxidation is equal to the current reduction.

$$i_{oxidation} - i_{reduction} = 0 \; at \; E_{corr} \quad (1)$$

The anodic and cathodic Tafel plots are described by the Tafel equation:

$$\eta = \beta \log \frac{i_{corr}}{i_{current}} \quad (2)$$

η = overvoltage, the difference between the potential of the specimen and the corrosion potential.

β = Tafel constant

$i_{current}$ = current at overvoltage η, mA.

i_{corr} = corrosion current density, mA/cm^2

From equation 2, the anodic and cathodic currents obey the Tafel equation:

$$\eta = \beta_a \log \frac{i_{oxidation}}{i_{corr}} \quad (3)$$

$$\eta = -\beta_a \log \frac{i_{reduction}}{i_{corr}} \quad (4)$$

Polarization resistance can be obtained by solving of equations 3 and 4.

$$\frac{\eta}{i_{Measure}} = \frac{\beta_a \beta_c}{2.3 \; i_{corr} \; (\beta_a + \beta_c)} \quad (5)$$

Rearrangement of equation 5 gives:

$$i_{corr} = \frac{\beta_a \beta_c}{2.3(\beta_a + \beta_c)} \frac{\Delta i}{\Delta E} \quad (6)$$

The corrosion current can be related directly to the corrosion rate through the following equation:

$$Corrosion \; Rate \; (MPY) = \frac{0.13 \; i_{corr} \; (E.W.)}{d} \quad (7)$$

ΔE/Δi = slope of the polarization resistance plot, where ΔE is expressed in volts and Δi expressed in mA.

β_a = Tafel constant at anodic current, volts / decade.

β_c = Tafel constant at cathodic current, volts / decade.

E.W. = equivalent weight of the corroding species, g.

d = density of the corroding species, g / cm^2.

MPY = milli-inches per year, 10^{-3} in / year.

Tafel plotting results of potentiodynamic polarization test as shown in Table 3. The chemical conversion coated specimen had E_{corr} value of -1390 V and an I_{corr} value of 2.15×10^{-6}. However, the sol-gel sealed specimen showed an E_{corr} value of -1.316 V and an I_{corr} value of 1.15×10^{-7}, indicating that it is relatively less corrosive. Especially, corrosion rate derived from I_{corr} value shows significantly reduces the corrosion tendency with sol-gel sealing.

3.5. SEM image of a cross-section of coating specimens

Fig. 7 shows cross-sectional images of chemical conversion and sol-gel sealed chemical conversion dual layer on the Mg alloy surface. It can be seen that many cracks developed on the chemical conversion coating

Table 3. Potentiodynamic polarization parameters of coating specimens

	E_{corr} (V)	I_{corr} (A/cm^2)	Corrosion rate (MPY)
Chemical conversion coating	-1.390	2.15×10^{-6}	1.95
Sol-gel sealed	-1.316	1.15×10^{-7}	0.1

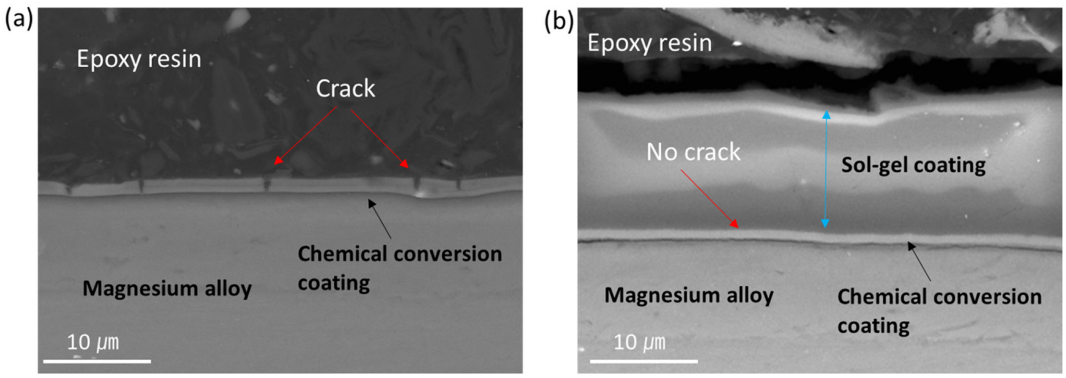

Fig. 7. The cross-section of SEM images of specimens. (a) chemical conversion coating and (b) sol-gel sealed specimen

layer. Therefore, as mentioned above, there is a strong possibility that corrosion factors can readily move to the metal surface. On the other hand, no crack was observed in the sol-gel sealed-chemical conversion coated specimen of Fig. 7b. This result is due to the sol-gel coating sealed all cracks on the chemical conversion coating layer. This result dictates good evidence to explain why the R_c value of the chemical conversion coating layer is higher than the R_s value of the sol-gel layer in the sol-gel sealed specimen.

4. Conclusions

The sol-gel coating and chemical conversion coating solutions were synthesized. The sol-gel sealed on chemical conversion coated magnesium alloy has been performed to observe its corrosion protection behavior. From SEM analysis, it was confirmed that many cracks formed in the chemical conversion process were well sealed with a sol-gel coating. In the thermal shock test, it was confirmed that the intensity of crack in the chemical conversion layer increased by thermal shock test but on dual-layer consist of sol-gel sealed specimen remained unaffected. The corrosion protection behavior with the thermal shock test was measured via electrochemical impedance spectrometer and potentiodynamic polarization test. Dual-layer of a sol-gel sealed specimen on chemical conversion showed a prolonged corrosion rate compared to only chemical conversion coating specimen. Therefore, it is confirmed that sol-gel coating on chemical conversion coating has a remarkable sealing effect and can have a breakthrough in overcoming the limitation on magnesium alloy used in engine blocks.

References

1. H. Dong, Z. Jin, H. Jinfeng, L. Yong, and H. Guangyu, A review on ignition mechanisms and characteristics of magnesium alloys, *Journal of Magnesium and Alloys*, **8**, 329 (2020). Doi: https://doi.org/10.1016/j.jma.2019.11.014
2. W. J. Joost and P. E. Krajewski, Towards magnesium alloys for high-volume automotive applications, *Scripta Materialia*, **128**, 107 (2017). Doi: https://doi.org/10.1016/j.scriptamat.2016.07.035
3. M. Easton, A. Beer, M. Barnett, C. Davies, G. Dunlop, U. Durandet, S. Blacket, T. Hilditch, and P. Beggs, Magnesium alloy applications in automotive structures, *JOM*, **60**, 57 (2008). Doi: https://doi.org/10.1007/s11837-008-0150-8
4. W. Gan, C. Liu, and F. Lu, Study on surface modification and properties of the AZ91D magnesium alloy used for automobile engine, *Journal of Materials Research and Technology*, Available online 4 May (2020). Doi: http://doi.org/10.1016/j.jmrt.2020.03.084
5. G. Song and D. H. Stjohn, Corrosion of magnesium alloys in commercial engine coolants, *Materials and Corrosion*, **56**, 15-23 (2005). Doi: https://doi.org/10.1002/maco.200403803
6. P. Zhou, B. Yu, Y. Hou, G. Duan, L. Yang, B. Zhang, T. Zhang, and F. Wang, Revisiting the cracking of chemical conversion coating on magnesium alloys, *Corrosion Science*, **178**, 109069 (2021). Doi: https://doi.org/10.1016/j.corsci.2020.109069
7. S. Liao, B. Yu, X. Zhang, X. Lu, P. Zhou, C. Zhang, X. Chen, T. Zhang, and F. Wang, New design principles for the bath towards chromate-and crack-free conversion coatings on magnesium alloys, *Journal of Magnesium and Alloys*, **9**, 505 (2021). Doi: https://doi.org/10.1016/j.jma.2019.12.013
8. D. Balgude and A. Sabnis, Sol–gel derived hybrid coatings as an environment friendly surface treatment for corrosion protection of metals and their alloys, *Journal of Sol-Gel Science and Technology*, **64**, 124 (2012). Doi: https://doi.org/10.1007/s10971-012-2838-z
9. J. Mosa, N. C. Rosero-Navarro, and M. Aparicio, Active corrosion inhibition of mild steel by environmentally-friendly Ce-doped organic–inorganic sol–gel coatings, *RSC Advances*, **6**, 39577 (2016). Doi: https://doi.org/10.1039/C5RA26094A
10. M. L. Zheludkevich, I. M. Salvado, and M. G. S. Ferreira, Sol–gel coatings for corrosion protection of metals, *Journal of Materials Chemistry*, **15**, 5099 (2005). Doi: https://doi.org/10.1039/B419153F
11. M. Whelan, J. Cassidy, and B. Duffy, Sol–gel sealing characteristics for corrosion resistance of anodised aluminium, *Surface and Coatings Technology*, **235**, 86 (2013). Doi: https://doi.org/10.1016/j.surfcoat.2013.07.018
12. V. R. Capelossi, M. Poelman, I. Recloux, R. P. B. hernandez, J. G. de Melo, and M. G. Oliver, Corrosion protection of clad 2024 aluminum alloy anodized in tartaric-sulfuric acid bath and protected with hybrid sol–gel coating, *Electrochimica Acta*, **124**, 69 (20140). Doi: https://

doi.org/10.1016/j.electacta.2013.09.004
13. J. Hu, Q. Li, X. Zhong, L. Zhang, and B. Chen, Composite anticorrosion coatings for AZ91D magnesium alloy with molybdate conversion coating and silicon sol–gel coatings, *Progress in Organic Coatings*, **66**, 199 (2009). Doi: https://doi.org/10.1016/j.porgcoat.2009.07.003
14. F. Mansfeld, Tafel slopes and corrosion rates from polarization resistance measurements, *Corrosion*, **29**, 397 (1973). Doi: https://doi.org/10.5006/0010-9312-29.10.397
15. R. Bandy, The simultaneous determination of tafel constants and corrosion rate—A new method, *Corrosion Science*, **20**, 1017 (1980). Doi: https://doi.org/10.1016/0010-938X(80)90081-5